TECHNICAL NOTE

NONLINEAR AERODYNAMIC MODELING OF CASCADE FINS AND DELTA-WING AIRCRAFT MODEL

Rakesh Kumar
Ph.D Student
Department of Aerospace Engineering
Indian Institute of Technology Kanpur
Kanpur-208 016, India
Email : rakpec@iitk.ac.in

Ajay Misra
Flight Lab Incharge
Department of Aerospace Engineering
Indian Institute of Technology Kanpur
Kanpur-208 016, India
Email : majay@iitk.ac.in

A.K. Ghosh
Professor
Department of Aerospace Engineering
Indian Institute of Technology Kanpur
Kanpur-208 016, India
Email : akg@iitk.ac.in

Abstract

The paper presents the modeling of the nonlinear longitudinal aerodynamics associated with the cascade fins and scale-down model of a delta-wing aircraft at high angles of attack. The Kirchhoff's steady-state stall model was used to model the stall characteristics and the Maximum Likelihood (ML) method was used to estimate the stall characteristic parameters. The cascade fin models with a rectangular and an airfoil (NACA-0012) cross-section were used to generate the variation of lift coefficient with angle of attack. The wind tunnel data pertaining to the cascade fin models were generated by varying the gap-to-chord ratios with and without end plates. The effect of end plates and the gap-to-chord ratio on the stall characteristics and the parameter estimation was analysed. The estimation results were compared to the reference results. In addition, the application of the Kirchhoffs steady-stall model to the scale-down model of a delta-wing aircraft has also been presented. The analysis pertaining to the cascade fins can be utilized as a basis for an initial design of cascade fins for guided missiles with desirable stall characteristics.

Nomenclature

a_1 = Static stall characteristics parameter
A = Aspect ratio
C_L = Lift coefficient
C_{L_o} = Lift coefficient at zero angle of attac
C_{L_α} = Lift curve slope, $(\partial C_L / \partial \alpha)$
S_{ref} = Reference area, m^2
$S_{exposed}$ = Exposed area, m^2
X = Describes the instantaneous location of an idealized flow separation point along the chord on the upper surface of the wing
X_0 = Steady-state flow separation point
α = Angle of attack, deg
α^* = Break point corresponding to X_0=0.5, deg
Λ = Sweep angle, deg
β = $\sqrt{1 - M^2}$,where M is Mach number
η = $C_{l_\alpha} / (2\pi)$, where C_{l_α} is two-dimensional lift curve slope

Abbreviations

AF, FP = Airfoil, Flat plate
EPY, EPN = With and without end plate
ML = Maximum Likelihood

Paper Code : V63 N4/731-2011. Manuscript received on 11 Oct 2010. Reviewed and accepted as a Technical Note on 12 Jul 2011

Introduction

Unsteady aerodynamics is one of the topics being investigated extensively. Under stationary attached flow conditions, aerodynamic effects can be adequately described using time-invariant parameters and linear models. But at higher angles of attack, the models are highly nonlinear due to dominant unsteady effects and flow separation [1-3]. The models based on computational fluid dynamics methods, wind tunnel tests and semi-empirical formulations provide a basis for analytical investigations of the complex flow phenomena, but postulating them in an analytical form suitable for parameter estimation is difficult. An alternative approach [4-5] to describe analytically the flow separation as a function of an internal state variable has been followed in the present study. Since the approach retains the state-space formulation, it is directly amenable to identification and validation from the flight data [6-8].

The grid fins, sometimes also called the lattice fins, are a relatively recent development in guided missile technology [9]. Unlike conventional planar fins, the grid fins do not experience classical 'stall' at high angles of attack and, hence, exhibit more effective stability and control characteristics at intermediate and large angles of attack [10-14]. The main drawback of the lattice fin is the high drag and low aerodynamic efficiency. Fig.1a shows the grid/lattice fins on a missile body whereas the application of the same has been shown in the Fig.1b.

A new category of grid fins, nomenclatured as 'Cascade fins' has been proposed by Misra [15] in order to increase the aerodynamic efficiency. A cascade fin has planar members placed parallel to each other at a distance based on an optimized gap-to-chord ratio (ratio of gap between the two fins to the chord of the fin). It is the absence of cross members that makes a cascade fin different from a grid fin. In cascade fin design, an appropriate selection of gap-to-chord (g/c) ratio and the number of planar members in the cascade lead to desirable stall angle and overall lift coefficient, respectively.

The wind tunnel data pertaining to cascade fin models generated by Misra [15] was used for modeling the nonlinear aerodynamics using the Kirchoff's steady-stall model [15-16] and estimate the stall characteristic parameters using the ML method [16]. The model geometries of cascade fins were having rectangular and NACA-0012 airfoil cross-sections. The wind tunnel data with and without end plates for different g/c ratios was used. The wind tunnel data pertaining to a scale-down model of delta-wing aircraft generated by Manoj [17] was also used for modeling the stall characteristics. The wind tunnel data consisting of the variation of lift coefficient (C_L) with angle of attack (α) were generated by conducting the experiments [15] in the National Wind Tunnel Facility (NWTF) in the department of Aerospace Engineering at the Indian Institute of Technology, Kanpur for both the cases.

In this paper, Section - Wind Tunnel Characteristics, Model Geometries and Experimental Set-up, describes the wind tunnel characteristics, schematic used to define the model geometries, the model geometries and experimental set-ups. In Section - The Used Wind Tunnel (WT) Data, presents the wind tunnel data pertaining to cascade fin models. Section - Steady-State Stall Modelling, outlines the Kirchhoff's steady-stall model. In Section - Results and Discussion deals with the application of the Kirchhoff's model and discussion of results. In Conclusion Section outlines the concluding remarks and scope for future work.

Wind Tunnel Characteristics, Model Geometries and Experimental Set-up

Wind Tunnel Characteristics

The experiments were conducted [15] in the NWTF in the Aerospace Engineering department at the Indian Institute of Technology, Kanpur. The NWTF is the state-of-the-art, 3m x 2.25m, low speed, closed circuit wind tunnel facility with a large number of associated equipment and instrumentation. It can attain contraction ratio of 9:1, the maximum wind speed of 90m/s and the Reynolds number of 6 million/m. It has been equipped with four screens to dampen out the turbulence along with the provision of an additional screen. It can measure the turbulence intensity level of less than 0.1%. The local deviation in the flow angularity is less than 0.1%. The NWTF is equipped with a single stage, twelve-bladed fan with a tip diameter of 4.64 m followed by a seven-bladed stator. The fan drive is powered by a 1000 kW (450 rpm) variable speed DC motor drive. The NWTF has been equipped with thyristor type digital DC drive to regulate the fan speed within ½ rpm.

A medium load range 6-component strain gage balance was used to measure the forces and moments acting on the models during the experiment. The schematic and actual load balance (BA 050_D60_L425) of Type-D has been shown in Fig.2. The load balance was 425mm long and was having maximum diameter of 60mm.

The load balance was having a sensitivity of 0.1%. The balance was made of stainless steel (17-4-PH) with yield strength of about 118 kg/mm^2. The balance consisted of the two normal-force gauge stations, the two side-force gauge stations, the two axial-force measuring bridges and one rolling moment bridge. The digital data acquisition system was used to obtain the wind tunnel data.

Schematic Used to Define the Model Geometries

The cascade fin model geometries were categorized in the two series. The terminologies 'FP series' and 'AF series' were used to define the cascade fin models with rectangular and NACA-0012 airfoil cross-section, respectively. The FP series models consisted of cascade fins with and without end plates having different g/c ratios whereas the AF series models consisted of cascade fins without end plates for different g/c ratios.

An alpha-numeric terminology was used to define the cascade fin model geometries. For example, in the terminology AA_BB_C.CD (FP_C4_0.5Y or AF_C4_0.5N), initial two characters (AA) define the series (FP or AF), the following two characters (BB) after underscore (_) define the number of planar fins in the cascade (C4), the next three characters (C.C) after underscore (_) represent the g/c ratio (0.5) and last character (D) defines the status whether the cascade is with or without end plate (Y and N are used for with and without end plate, respectively). Tables-1 to 3 and Table-4 can be used to understand the nomenclature used to define the model geometries of the FP series and the AF series, respectively.

Model Geometries

The cascade fin model geometries having a rectangular and an airfoil (NACA-0012) cross-section were tested in the NWTF. The FP series models were tested with and without end plates having different g/c ratio whereas AF series models were tested without end plates for different g/c ratios having four fins in the cascade. The model geometry for each case such as FP series (EPY and EPN) and AF series are shown in Figs. 3(a-b) and 4, respectively. The other model geometries [15] pertaining to the FP Series and the AF Series were having similar configurations.

Figures 3a and 3b present the schematic of the model geometries for the FP series with and without end plates, respectively. The shown model geometries consisted of four fins in the cascade having g/c ratio of 0.5. The figures also show the other geometrical parameters of the models such as length (0.2 m), chord (0.1 m) and thickness of base plate (0.002 m) and end plate (0.002 m). The FP series models with other values of g/c chord ratios (0.6-0.9) were having similar geometries.

Figure 4 presents the schematic of the AF series model (NACA-0012) without end plate for the g/c ratio of 0.5. The AF series models consisted of four planar fins in the cascade. The figure also shows the other geometrical parameters such as the length (0.2 m), chord (0.1 m) and maximum thickness (0.012 m). The thickness of the base plate was 0.002 m. The AF series models with other values of g/c chord ratios (0.6-0.9) were having similar geometries.

The delta-wing aircraft model shown in Fig. 5 was tested in the NWTF to generate the wind tunnel data. The composite material was used to fabricate the aircraft model. The model consisted of the two elevon control surfaces for the longitudinal (when used collectively) and the lateral (when used differentially) control. Each elevon was having rectangular geometry (0.038m x 0.375m). The vertical tail of the aircraft model consisted of one rudder with additional four fins (two on the starboard side and two on the port side of wing).

Table-1 presents the values of various geometrical parameters pertaining to the delta-wing aircraft model.

Table-1 : Geometrical Parameters of the Delta-Wing Aircraft

Quantity	Wing	Horizontal Tail
Mean aerodynamic chord (m)	0.31	0.075
Root chord (m)	0.43	0.075
Tip chord (m)	0.14	0.075
Span (m)	1.18	1.05
Planform area (m^2)	0.336	0.079
Aspect ratio	4.14	14.0
Taper ratio	0.326	1.0
Sweep (deg)	26.17°	0°

Experimental Set-ups

Figure 6 shows the schematic of experimental set-ups used for the cascade fin models (FP series and AF series). The models were mounted on the balance which was fixed vertically on a turn table of the wind tunnel floor through a front and a rear end adaptor. A shroud was placed over the balance, the front end and the rear end adaptor to isolate the balance from direct wind loads.

Figure 7a shows the rear view of the schematic of the models with and without end plate for the FP series having the five fins in the cascade whereas the schematic of models without end plates for the AF series has been shown in Fig.7b for the four fins in the cascade when placed in the test section during the wind tunnel testing. A digital data acquisition system was used to obtain the wind tunnel data. The used wind tunnel data was obtained at V=40 m/s simulating the Reynolds number of 253000/m using non-dimensional length of 0.2. The density of air was taken to be 1.2 kg/m^3 for the computation of the dynamic pressure and the Reynolds number.

The two experimental set-ups were used during the conduct of the experiments using the delta-wing aircraft model in the NWTF. The first set-up consisted of the adapter attached to the load balance as well as to the delta-wing aircraft model (Fig.8a) whereas in the second set-up, the adapter was attached only to the load balance (Fig.8b).

A cylindrical adapter (Figs.8a and 8b) was used to interconnect the aircraft model and the load balance inside the working section of the wind tunnel. The lower end of the adapter was attached at the top of the load balance whereas the upper end of the adapter was attached at the bottom of the aircraft model.

The Used Wind Tunnel (WT) Data

WT Data: FP Series

In case of the FP series, the tests were conducted by varying the g/c ratio with and without end plates to see the effect on the modeling and estimation. Figs.9a and 9b present the variation of C_L with α for the FP series models having different g/c ratios (0.5 - 0.9) with and without end plates, respectively.

It can be observed (Fig. 9(a-b)) that the variation of C_L with α is fairly linear upto an angle of attack of 15 degrees but becomes nonlinear beyond 15 degrees. In case of FP seires models with end plates, higher $C_{L_{max}}$ is achieved at lower stalling angle (α_{stall}) as compared to FP series models without end plates. An increase in $C_{L_{max}}$ and decrease in (α_{stall}) can be observed with increase in the g/c ratio in case of the FP series models with end plates whereas an increase in $C_{L_{max}}$ with an almost constant (α_{stall}) can be observed with increase in the g/c ratio in case of the FP series models without end plates.

WT Data: AF Series

In case of the AF series models, the wind tunnel tests were conducted by varying the g/c ratio (0.5 - 0.9) without end plates. Fig.10 presents the variation of C_L with α for the AF series models having different g/c ratios without end plates. It can be observed (Fig.10) that the linear portion of the variation of C_L with α kept on decreasing with increase in g/c ratio. An increase in $C_{L_{max}}$ and decrease in (α_{stall}) can be observed with increase in g/c ratio. An erratic behavior near stall (increase in $C_{L_{max}}$ following a dip after stall) can also be observed.

WT Data: Delta-wing Aircraft Model

In case of delta wing aircraft model, the experiments were performed at a subsonic speed of 20 m/s. The average Reynolds number of 2×10^6 based on the wing span of the aircraft model was used. The angle of attack of the delta-wing aircraft model was varied up to 40 deg in a step of 5 deg. The forces and the moment generated by using the experimental set-up shown in Fig.8b were deducted from the corresponding forces and moment generated by using the experimental setup shown in Fig.8a. This was done to exclude the aerodynamic effects of the adapter and the load balance from the wind tunnel data.

The wind tunnel data (Fig.11) pertaining to the delta-wing aircraft model consisted of the variation of the lift coefficient (C_L), the drag coefficient (C_D) and the moment coefficient (C_m) as a function of angle of attack (α). However, the variation of the lift coefficient (C_L) was used to model the stall characteristics. The coefficients of lift, drag and moment at zero angle of attak ($C_{L_o} = 0.0501$, $C_{D_o} = 0.0606$ and $C_{m_o} = 0.0435$) the linear lift and pitching moment curve slopes (C_{L_α} = 3.73/rad and C_{m_α} = 0.7207/rad) can be obtained from the generated wind

tunnel data. It can also be observed that the aerodynamic stall of the delta-wing aircraft model occurs at an angle of attack of 15°.

All the sets of the wind tunnel data were used to validate the Kirchhoff's steady-stall model for modeling the nonlinear aerodynamics (stall characteristics) and to estimate the stall characteristic parameters.

Steady-state Stall Modeling

Aerodynamic models become highly nonlinear due to dominant unsteady effects and flow separation at high angles of attack. For such a case, based on Kirchhoff's theory of flow separation for a symmetrical profile, the lift can be modeled as a function of angle of attack (α) and flow separation point [16].

$$C_L(\alpha, X) = C_{L_\alpha}\left\{\frac{1+\sqrt{X}}{2}\right\}^2 \alpha \qquad (1)$$

where C_{L_α} is lift curve slope and is given as

$$C_{L_\alpha} = \frac{(2\pi A)}{\left(2+\sqrt{4+\frac{A^2\beta^2}{\eta^2}(1+\frac{\tan^2\Lambda}{\beta^2})}\right)} * \frac{S_{exposed}}{S_{ref}} \qquad (2)$$

Reformulating the Kirchhoff's formulation of flow separated lift (Eq. (1)) and extending by C_{L_α} for non-symmetrical profile yields the following expression for steady state profile of flow separation point (Xo)

$$Xo = \left\{2\sqrt{[(C_L - C_{L_o})/(C_{L_\alpha}\alpha)]} - 1\right\}^2 \qquad (3)$$

The steady flow separation point (Xo) depends upon the airfoil and wing configuration. Using Eq.(1) with X = Xo the function can be determined statically in wind tunnel by substituting the values of C_{L_α}, C_{L_o} and C_L obtained through wind tunnel testing. It may be noted that the values of C_{L_α} required in Eq.(3) corresponds to linear value of the lift curve slope. An alternative procedure has been used in this work wherein Xo has been modeled as per Eq. (4).

$$Xo = \frac{1}{2}\left\{1 - \tan h\left[a_1(\alpha - \alpha^*)\right]\right\} \qquad (4)$$

where a_1 defines the static stall characteristics of the airfoil and α^* is the breakpoint corresponding to Xo = 0.5. This approximation is better suited to parameter estimation because it is a continuous function in its entire range and has just two unknown parameters, namely a_1 and α^*. The values of parameters a_1 and α^* can be estimated by maximum likelihood method using Eq.(4).

Results and Discussion

The Kirchhoff's steady stall model was applied to model the stall characteristics using the wind tunnel data pertaining to the model geometries of the FP series and the AF series. The flow separation point was calculated using Eq.(3). The values of C_L at given α was read directly from the wind tunnel generated data. The value of C_{L_α} required to compute Xo was computed by using Vortex Lattice Method [15]. The calculated value of Xo, thus obtained, was referred to as $Xo_{(WT)}$. The computed flow separation point using Eq.(4) was referred to as $[Xo_{(computed)}]$. The ML method was applied to minimize the error between the calculated $[Xo_{(WT)}]$and the computed $[Xo_{(computed)}]$ value of flow separation point and estimate the stall characteristic parameters (a_1 and α^*). The Cramer-Rao bounds were also computed along with the stall characteristic parameters to assess the level of accuracy of the estimates.

For the sake of more clearity in the discussion of results, the flow separation point (Xo) generated for different values of a_1 and α^*as a function of angle of attack has been shown in Fig.12 for a single fin model having NACA-0012 airfoil section. The wind tunnel data generated by Misra [15] for NACA-0012 airfoil section was used to generate Fig.12. First, the value of a_1 (6.0, 7.5 and 9) was varied by keeping α^* (0.3 radian) constant. Next, the value of α^* (0.2, 0.3 and 0.4) was varied by keeping a_1 (7.5) constant. It can be seen that break point occurs at lower angle of attack when α^* is having a lower value whereas the curve tends to straighten more horizontally for the lower value of a_1 signifying the lower $C_{L_{max}}$ with improved stall characteristics.

Cascade Fins: FP Series

The wind tunnel data pertaining to the FP series models were used to estimate the stall characteristic parameters (a_1 and α^*) using the ML method. Table-2 presents the estimated values of a_1 and α^* along with the Cramer-Rao

Table-2 : Effect of g/c Ratio on Parameter Estimation : FP Series (EPY)

Fin Configuration	Gap-to-Chord Ratio	Model Estimated		Ref. [15] Estimated	
		a_1	α^* (deg)	a_1	α^* (deg)
FP_C4_0.5 Y	0.5	6.25 (0.049)	25.6 (0.0007)	5.43	25.4
FP_C4_0.6 Y	0.6	6.09 (0.047)	25.4 (0.0007)	5.51	26
FP_C4_0.7 Y	0.7	5.3014 (0.0387)	24.5 (0.0008)	5.51	25.7
FP_C4_0.8 Y	0.8	5.11 (0.036)	23.3 (0.0008)	5.55	25
FP_C4_0.9 Y	0.9	6.78 (0.055)	22.9 (0.0007)	6.16	23.7

( ) Cramer-Rao Bounds

bounds for the FP series model with end plates for different g/c ratios. The g/c ratio was varied from 0.5 to 0.9 at an increment of 0.1.

It can be observed from Table-2 that the value of parameter α^* keeps on decreasing with increase in g/c ratio leading to break point at lower angle of attack. Also, the value of parameter a_1 keeps on decreasing with increase in g/c ratio (except for the value corresponding to g/c ratio of 0.9), leading to the higher $C_{L_{max}}$. It can be seen that the estimated results compare well with the reference results [15].

Figure 13 shows the flow separation point (*X*o) generated by using the estimated stall characteristic parameters (a_1 and α^*) as a function of angle of attack for FP series models with end plates for different g/c ratios.

It can be observed from the figure that the optimum condition exist in-between the two extremes giving the optimum break point, the higher $C_{L_{max}}$ with reasonably good stall characteristics.

Table-3 presents the estimated values of a_1 and α^* along with the Cramer-Rao bounds for the FP series model without end plates for different g/c ratios. It can be observed that the values of α^* and a_1 keep on decreasing with increase in g/c ratio leading to flow separation (break point) at lower angle of attack and higher $C_{L_{max}}$. It can also be observed that the values of a1 given in Table-2 (EPY) are relatively lower than in Table-3 (EPN), indicating relatively a higher value of $C_{L_{max}}$.

Figure 14 shows the flow separation point (*X*o) generated by using the estimated stall characteristic parameters (a_1 and α^*) as a function of angle of attack for FP series models without end plates for different g/c ratios. It can be observed from the figure that the optimum condition exist in-between the two extremes giving the optimum break point and reasonably high $C_{L_{max}}$ with good stall characteristics.

Table-3 : Effect of g/c Ratio on Parameter Estimation : FP Series (EPN)

Fin Configuration	Gap-to-Chord Ratio	Model Estimated	
		a_1	α^* (deg)
FP_C4_0.5 N	0.5	7.084 (0.059)	23.8 (0.0007)
FP_C4_0.6 N	0.6	6.416 (0.051)	25.2 (0.0007)
FP_C4_0.7 N	0.7	5.277 (0.038)	23.9 (0.0008)
FP_C4_0.8 N	0.8	5.249 (0.038)	23.2 (0.0008)
FP_C4_0.9 N	0.9	4.167 (0.028)	20.4 (0.0009)

( ) Cramer-Rao Bounds

Next, the validation exercise was carried out for the FP series models. The computed flow separation point using the estimated stall characteristic parameters for the FP series models were used to model the lift coefficient (C_L). Figs.15(a-b) present the modeled C_L for the FP series with and without end plates for different g/c ratios. The effect of variation of the g/c ratio can be observed as the extent of departure of the modeled C_L from the wind tunnel calculated C_L increases at higher angles of attack with increases in the g/c ratio. The increase in departure at

higher angles of attack may be due to inability of the Kirchhoff's steady-stall model to capture the complex separation phenomenon at high angles.

Cascade Fins: AF Series

The wind tunnel data pertaining to the AF series models were used to estimate the stall characteristic parameters (a_1 and α^*) using the ML method. Table-4 presents the estimated values of a_1 and α^* along with the Cramer-Rao bounds for the AF series models without end plates for different g/c ratios. The g/c ratio was varied from 0.5 to 0.9 at an increment of 0.1.

It can be observed from Table-4 that the value of parameter a1 keeps on decreasing with increase in g/c ratio (except for the value corresponding to g/c ratio of 0.9), leading to higher $C_{L_{max}}$. The value of parameter α^* shows the fluctuating behavior with a maximum value corresponding to g/c ratio of 0.5. It can be seen that the estimated results compare well with the reference results [15].

Figure 16 shows the flow separation point (Xo) generated by using the estimated stall characteristic parameters (a_1 and α^*) as a function of angle of attack for AF series models without end plates for different g/c ratios. It can be observed from the figure that the break point corresponding to g/c ratio of 0.5 occurs at maximum value of angle of attack whereas the optimum condition for a reasonably high value of $C_{L_{max}}$ with good stall characteristics exist in-between the two extremes.

Similarly, the validation exercise was carried out for the AF series models. The computed flow separation point using the estimated stall characteristics parameters for the AF series models were used to model the C_L. Fig.17 present the modeled C_L for the AF series without end plates for different g/c ratios. The effect of variation of the g/c ratio can be observed as the extent of departure of the modeled C_L from the wind tunnel calculated C_L increases at higher angles of attack with increases in the g/c ratio.

Delta-wing Aircraft Model

The Kirchhoff's steady-stall model was applied to the wind-tunnel data pertaining to the delta-wing aircraft model for modeling the flow separation point (Xo) and estimate the stall characteristic parameters (a_1 and α^*) using the ML method. The flow separation point computed by using Eq.(3) was referred to as $Xo_{(WT)}$. The flow separation point computed by using Eq.(4) was referred to as $[Xo_{(computed)}]$. The ML method was used to minimize the error between the measured $[Xo_{(WT)}]$ and computed $[Xo_{(computed)}]$ value of flow separation point and estimate the stall characteristic parameters [a_1 and α^*].

Figures 18 presents the wind tunnel measured $[Xo_{(WT)}]$ and model estimated $[Xo_{(computed)}]$ flow separation point as a function of α during the estimation of a_1 and α^* using the ML method for delta-wing aircraft model.

Table-5 presents the estimated values of a_1 and α^* along with their Cramer-Rao bounds from wind tunnel data of pertaining to delta-wing aircraft models using ML method.

Figure 19 presents the comparison of the wind-tunnel data generated C_L and the C_L generated by using the estimated stall characteristics parameters. A well matched variation of wind tunnel generated and model estimated C_L as a function of α validates the estimation.

Table-4 : Effect of g/c Ratio on Parameter Estimation : AF Series (EPN)

Fin Configuration	Gap-to-Chord Ratio	Model Estimated		Ref. [15] Estimated	
		a_1	α^* (deg)	a_1	α^* (deg)
AF_C4_0.5 N	0.5	9.15 (0.480)	27.7 (0.003)	10.18	29
AF_C4_0.6 N	0.6	8.46 (0.427)	27.5 (0.003)	8.8	27.75
AF_C4_0.7 N	0.7	8.20 (0.565)	25.4 (0.003)	7.62	25.75
AF_C4_0.8 N	0.8	8.05 (0.396)	26.3 (0.003)	7.04	26.5
AF_C4_0.9 N	0.9	9.72 (0.526)	25.6 (0.003)	8.12	25.5
( ) Cramer-Rao Bounds					

Table-5 : Estimated Stall Characteristic Parameters : Delta-Wing Aircraft Model	
Parameters	Model Estimated
a_1	8.62 (1.835)
α^* (deg)	14.25 (0.021)
( ) Cramer-Rao Bounds	

Conclusion

The paper presents the application of the Kirchhoff's steady-stall model to the longitudinal wind tunnel data for modeling the stall characteristics of the cascade (FP series and AF series) fin models having rectangular and airfoil cross-section (NACA-0012) and the delta-wing aircraft model. The effect of variation of the gap-to-chord ratio and the end plates on the stall characteristics was analysed. The estimated results were presented in the graphical as well as in the tabular form. In most of the cases, the results obtained using the Kirchhoff's model were found better than the reference [15] results.

It was observed that increase in the g/c ratio resulted in the higher value of the maximum lift coefficient with reasonably good stall characteristics but also resulted in the break points (flow separation) at lower angles of attack. The end plates resulted in a higher value of the maximum lift coefficient due to the end plate effects (as observed in the case of aircraft). Therefore, the desirable stall angle and overall lift characteristics can be obtained by an appropriate selection of the gap to chord ratio with/without end plates. The Kirchhoff's steady-stall model was also applied successfully to the wind tunnel data of the delta-wing aircraft model for modeling the stall characteristics. Hence, it can be concluded that the Kirchhoff's steady-state stall model could be used suitably to capture the nonlinear cascade fin aerodynamics.

The work has been presented for the steady-state case of wind tunnel using the Kirchhoff's steady stall model; however, the Kirchhoffs quasi-steady stall model can be applied to the real flight data of guided missiles with tail having the cascade fins to model nonlinear aerodynamics. The Kirchhoff's quasi-steady stall model [16] can be applied to the real flight data of any aircraft to model the nonlinear aerodynamics at high angles of attack.

References

1. Klein, V. and Noderer, K.D., "Modeling of Aircraft Unsteady Aerodynamic Characteristics, Part-1 : Postulated Models", NASA TM-109120, May, 1994.

2. Klein, V., "Modeling of Longitudinal Unsteady Aerodynamic of a Wing-tal Combination", NASA CR-1999-209547, September, 1999.

3. Abramov, N., Goman, M. and Khrabrov, A., "Aircraft Dynamics at High Incidence Flight with Account of Unsteady Aerodynamic Effects", AIAA Paper, 2004-5274, 2004.

4. Leishman, J.G. and Nguyen, K.Q., "State-space Representation of Unsteady Airfoil Behavior", AIAA Journal, Vol.28, No.5, 1990.

5. Goman, M. and Khrabrov, A., "State-space Representation of Aerodynamic Characteristics of an Aircraft at High Angles of Attack", Journal of Aircraft, Vol.31, No.5, 1990.

6. Fischenberg, D., Identification of an Unsteady Aerodynamic Stall Model from Flight Test Data, AIAA Paper, 95-3438, Aug. 1995.

7. Greenwell, D.I., "A Review of Unsteady Aerodynamic Modeling for Flight Dynamics of Manoeuvrable Aircraft", AIAA Paper, 2004-5276, August, 2004.

8. Fischenberg, D. and Jategaonkar, R. V., "Identification of Aircraft Stall Behavior from Flight Test Data", RTO-MP-11, Paper No.17, March, 1999.

9. Fleeman, E. L., "Tactical Missile Design", AIAA Education Series, 2001.

10. Simpson, G. M. and Sadler, A. J., "Lattice Controls: A Comparison with Conventional Planar Fins", Proceedings of the NATORTO Applied Vehicle Technology Panel Symposium on Missile Aerodynamics, RTO-MP-5, NATO Research and Technology Organization, pp. (9-1)-(9-10), 1998.

11. Belotserkovskiy, S. M. et al., "Wings with Internal Framework", Machine Translation, FTD-ID (RS)-1289-86. Foreign Technology Division, February, 1987.

12. Washington, W. D. and Miller, M.S., "Grid Fins-A New Concept for Missile Stability and Control", AIAA Paper 93-0035, Reston, VA, January, 1993.

13. DeSpirito, J., Edge, L.H., Weinacht, P., Sahu, J. and Dinavashi, S., "Computational Fluid Dynamics Analysis of Missile with Grid Fins", Journal of Spacecraft and Rockets, Vol.38, No.5, September-October, 2001.

14. Washington, W.D. and Miller, M.S., "Experimental Investigation of Grid Fin Aerodynamics: A Synopsis of Nine Wind Tunnel and Three Flight Tests", Symposium on "Missile Aerodynamics", Sorrento, Italy, 11-14 May, 1998.

15. Misra A., "Investigation of Grid and Cascade Fins for Missile Flight Stabilization and Control", Ph.D. Thesis, Indian Institute of Technology, Kanpur, April, 2009.

16. Jategaonkar, R. V., "Flight Vehicle System Identification - A Time Domain Methodology", AIAA Progress in Aeronautics and Astronautics, Vol.216, AIAA, Reston, VA, August, 2006.

17. Manoj, K., "Design of 5 Degrees-of-freedom Dynamic Test Rig for Aerodynamic Characterization of Flight Vehicle", M.Tech Thesis, Indian Institute of Technology, Kanpur, May, 2010.

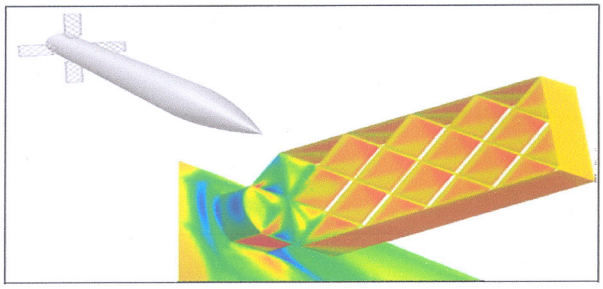

Fig.1a Grid Fins on Missile Body and a Close-up of the Grid/Lattice Fin [15]

Fig.1b Massive Ordnance Air Blast Bomb [9]

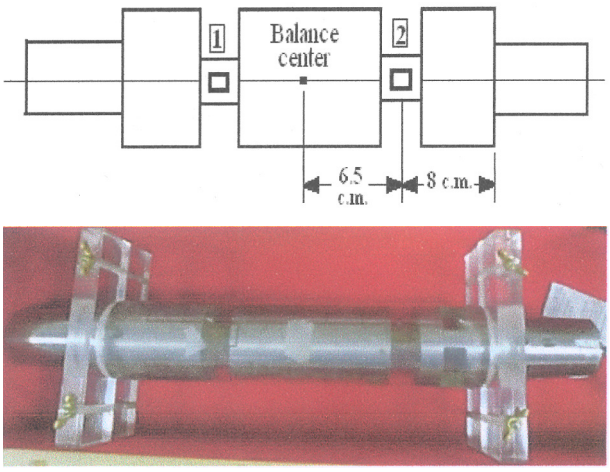

Fig.2 Schematic and the Actual Load Balance of Type-D

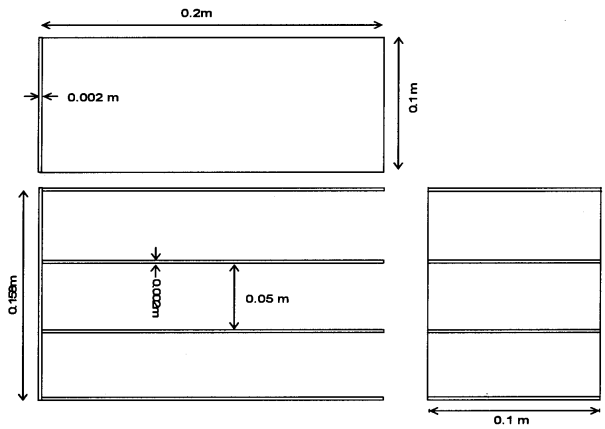

Fig.3a Schematic of the Model Geometry of the FP Series : FP_C4_0.5 N

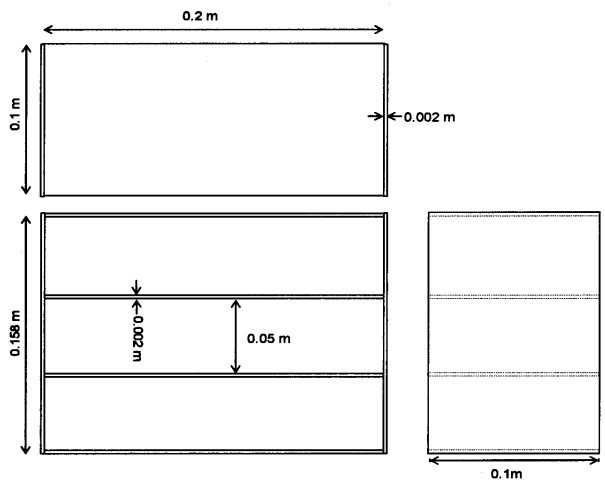

Fig.3b Schematic of the Model Geometry of the FP Series : FP_C4_0.5 Y

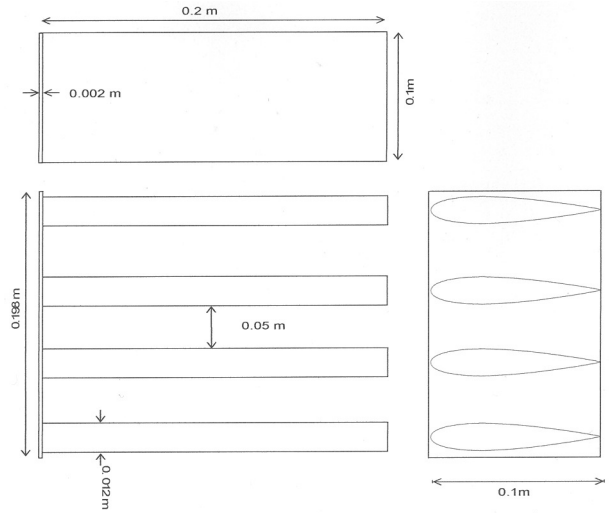

Fig.4 Schematic of the Model Geometry of AF Series : AF_C4_0.5 N

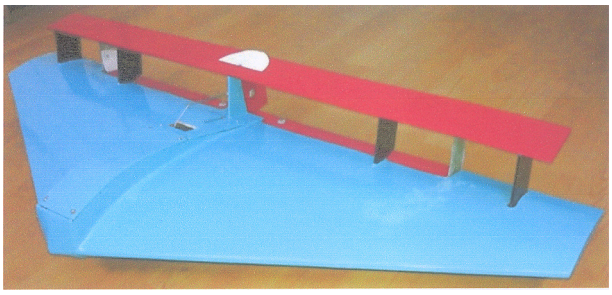

Fig.5 Delta-Wing Aircraft Model

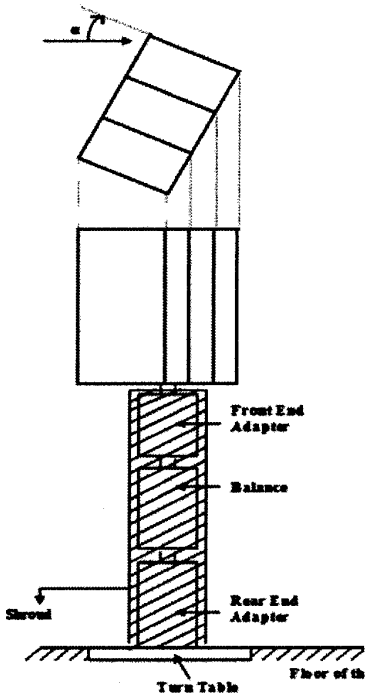

Fig.6 Experimental Set-up: AF and FP Series

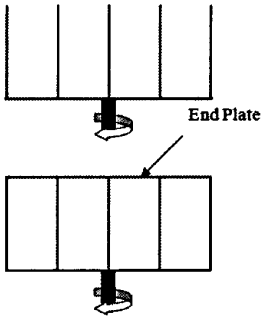

Fig.7a Schematic of FP Series (EPN and EPY) (Rear View at α = 0

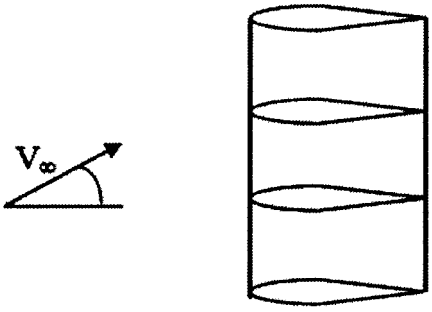

Fig.7b Schematic of AF Series

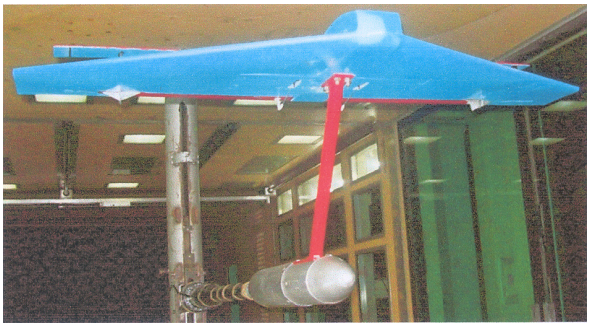

Fig.8a Experimental Setup of Delta-Wing Aircraft Model Inside NWTF

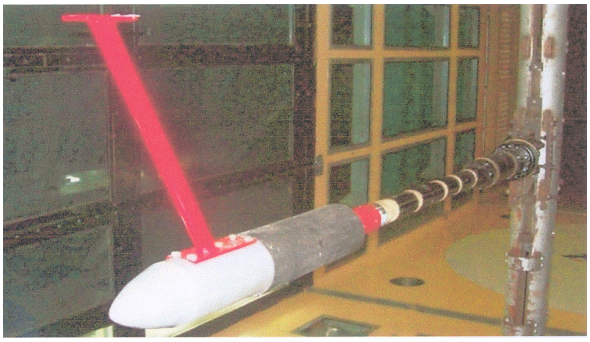

Fig.8b Adapter Mounted on the Load Balance

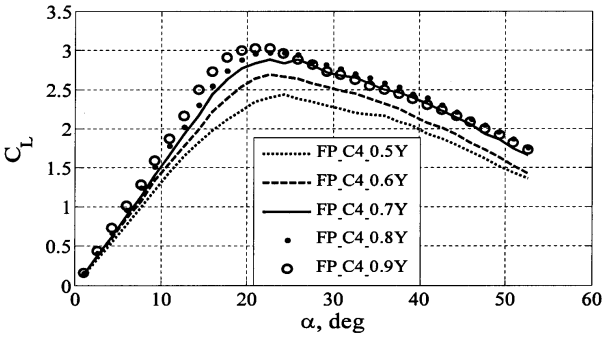

Fig.9a Variation of C_L with α; FP Series with Different g/c Ratios (EPY)

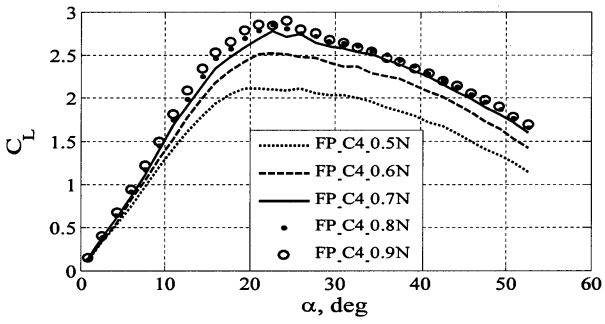

Fig.9b Variation of C_L with α: FP Series for Different g/c Ratios (EPN)

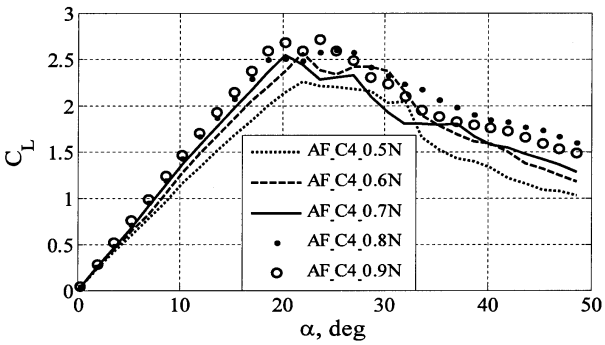

Fig.10 Variation of C_L with α; AF Series with Different g/c Ratios (EPN)

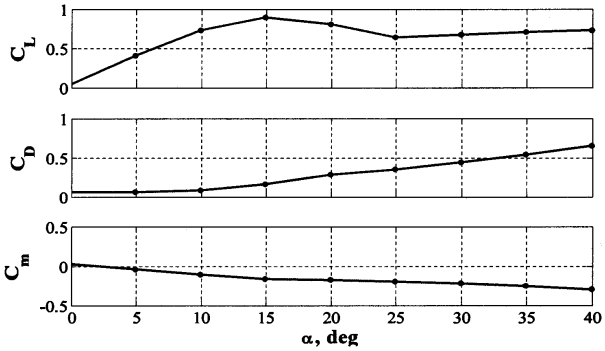

Fig.11 Variation of C_L, C_D and C_m with α; Delta-Wing Aircraft Model

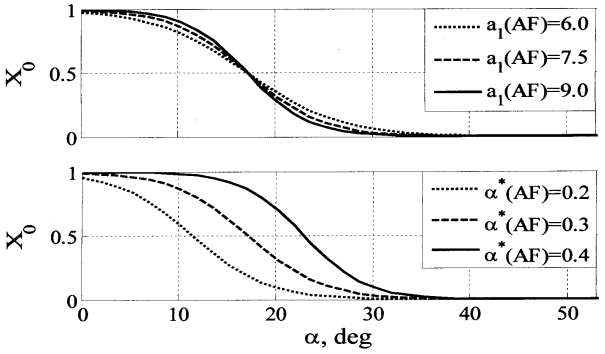

Fig.12 Variation of X_o with α for Different a_1 and α; Single Fin Model*

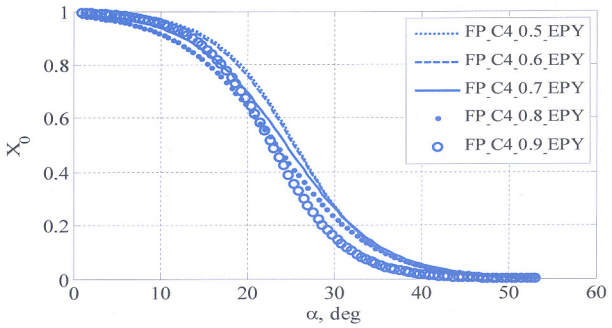

Fig.13 Variation of X_o with α for Different g/c Ratios; FP Series Models (EPY)

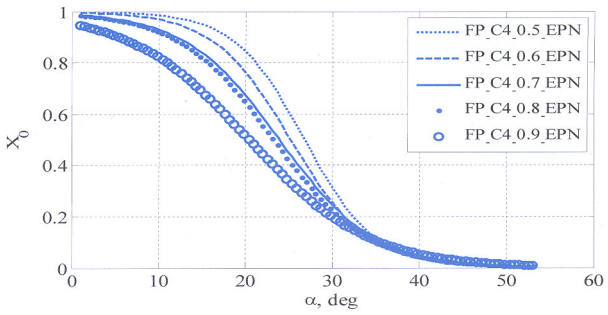

Fig.14 Variation of X_o with α for Different g/c Ratios; FP Series Models (EPN)

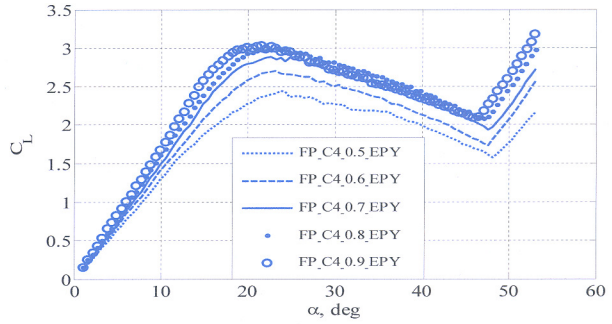

Fig.15a The Modeled C_L Using Computed X_o for Different g/c Ratios; FP Series (EPY)

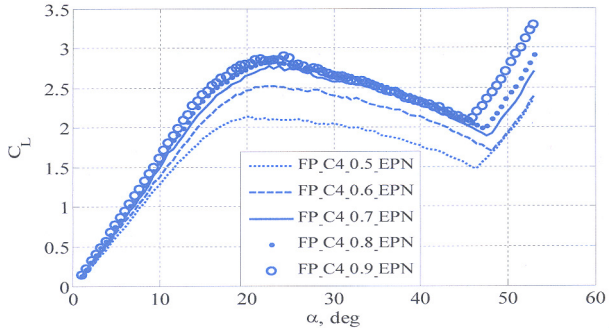

Fig.15b The Modeled C_L Using Computed X_o for Different g/c Ratios; FP Series (EPN)

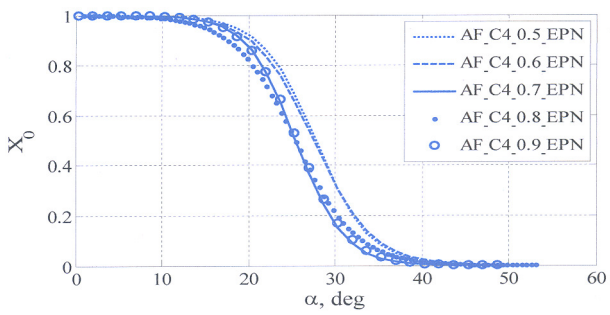

Fig.16 Variation of X_o with α for Different g/c Ratios; AF Series Models (EPN)

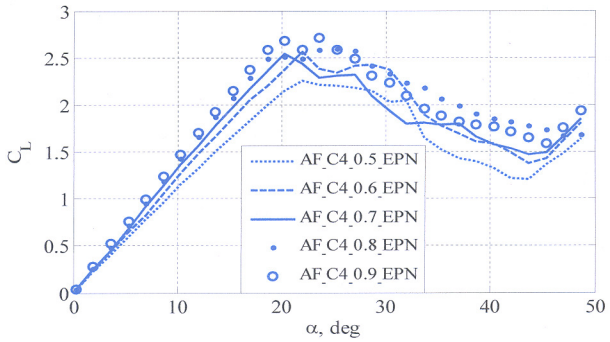

Fig.17 The Modeled C_L Using Computed X_o for Different g/c Ratios; AF Series (EPN)

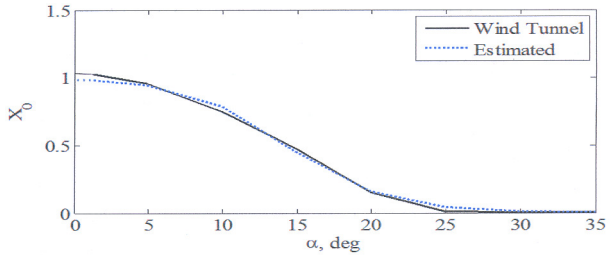

Fig.18 WT Measured and Model Estimated X_o; Delta-Wing Aircraft Model

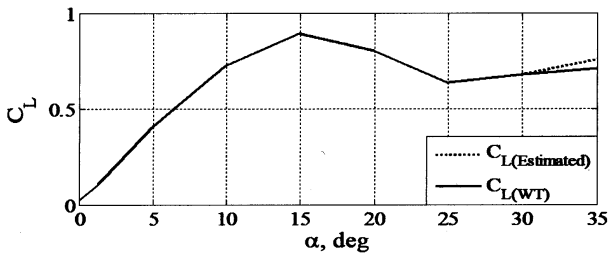

Fig.19 WT Measured and Model Estimated C_L; Delta-Wing Aircraft Model